THE ASTRONOMICAL JOURNAL, 116:1886–1896, 1998 October

A HIGH-RESOLUTION RADIO SURVEY OF THE VELA SUPERNOVA REMNANT

D. C.-J. BOCK
Radio Astronomy Laboratory, University of California, Berkeley, CA 94720; and School of Physics, University of Sydney, NSW 2006, Australia; dbock@astro.berkeley.edu

AND

A. J. TURTLE AND A. J. GREEN
School of Physics, University of Sydney, NSW 2006, Australia; turtle@physics.usyd.edu.au, agreen@physics.usyd.edu.au
Received 1998 May 5; revised 1998 June 26

ABSTRACT

This paper presents a high-resolution radio continuum (843 MHz) survey of the Vela supernova remnant. The contrast between the structures in the central pulsar-powered nebula of the remnant and the synchrotron radiation shell allows the remnant to be identified *morphologically* as a member of the composite class. The data are the first of a composite remnant at spatial scales comparable with those available for the Cygnus Loop and the Crab Nebula, and make possible a comparison of radio, optical, and soft X-ray emission from the resolved shell filaments. The survey, made with the Molonglo Observatory Synthesis Telescope, covers an area of 50 deg^2 at a resolution of $43'' \times 60''$, while imaging structures on scales up to $30'$.

Key words: ISM: individual (Vela SNR, Vela X) — pulsars: individual (PSR B0833−45) — supernova remnants

1. INTRODUCTION

The Vela supernova remnant (G263.9−3.3) is one of the closest and brightest supernova remnants (SNRs). Recent measurements support a distance of about 350 pc (Dubner et al. 1998 and references therein). Estimates of its age range from a few thousand years (Stothers 1980) to 29,000 yr (Aschenbach, Egger, & Trümper 1995) with a widely used value being that given by the characteristic age of its pulsar, 11,400 yr (Reichley, Downs, & Morris 1970). Its brightness and large angular size ($\sim 8°$) have made possible its study at many wavelengths. Yet it has been less intensively studied than other close remnants such as the plerionic Crab Nebula and the shell-type Cygnus Loop, although it is arguably the closest and a key member of the third major class of SNRs, the composite remnants. Among many controversies surrounding its nature has been that of whether it is a shell or a composite remnant. This paper aims to show that the Vela SNR definitely can be seen as a composite remnant on morphological grounds and should be considered the Galactic archetype.

Previous radio studies of the Vela SNR region have mainly used lower resolution single-dish images over a frequency range from 408 MHz to 8.4 GHz (Milne 1968a; Day, Caswell, & Cooke 1972; Milne 1980; Milne 1995; Duncan et al. 1996). The earliest observations showed the Vela SNR to comprise three main areas of radio emission, called Vela X, Y, and Z, within a diameter of 5°, corresponding roughly with the bright, filamentary structure of the nebula Stromlo 16 (Gum 1955; Milne 1968b). Until recently, this 5° diameter was thought to indicate the extent of the remnant, with the nebula Vela X containing the pulsar (PSR B0833–45), offset to one side. This pulsar, discovered in 1968, was immediately associated with the Vela SNR (Large, Vaughan, & Mills 1968). Calculations by Bailes et al. (1989) indicate that there is only a 0.1% probability that the pulsar and the supernova remnant are in chance superposition. Kundt (1988) deduced from the 408 MHz survey of Haslam et al. (1982) that the Vela SNR might be much larger, in fact about 8° across, with the pulsar approximately at the center. *ROSAT* and radio observations (Aschenbach 1992; Duncan et al. 1996) reinforced this model. The discovery that the speed and direction of the pulsar's proper motion indicate that it was born near the center of the 8° Vela SNR shell (Aschenbach et al. 1995) solves the offset problem. This is one of only a few reliable SNR/pulsar associations (Kaspi 1996). The most recent single-dish observations (Milne 1980; Milne 1995) began to resolve Vela X at higher frequencies (5–8.4 GHz) and uncovered strongly linearly polarized structure. Higher resolution observations at 327 MHz with the Very Large Array (VLA) by Frail et al. (1997) showed a bright filament near the center of Vela X, near the X-ray feature called a "jet" by Markwardt & Ögelman (1995). This feature extends southward from the pulsar, which is offset to the north of Vela X.

The radio spectral index of Vela X is flatter than that of the rest of the remnant, leading to the remnant's classification as a composite, with the Vela X nebula directly powered by the Vela pulsar (Dwarakanath 1991; Weiler & Sramek 1988). This conclusion has been controversial (Weiler & Panagia 1980; Milne & Manchester 1986; Weiler & Sramek 1988). The Vela SNR lies close to the Galactic plane, leading to difficulties in estimating the base level in both single-dish and interferometer images. To provide the first evidence supporting the classification as a composite on morphological grounds, radio observations are presented in this paper at the highest resolution yet used to image the Vela X region. A subsequent paper will present a multiwavelength study of Vela X and consider the nature of the central plerion in detail.

These are the first high-resolution radio observations to cover a large fraction of the entire Vela SNR, and are the first radio observations of the Vela shell at a resolution compatible with currently available optical and X-ray images. Radio observations of the Vela shell published before the present work have been at relatively low resolution. For example, the observations of Duncan et al. (1996) have a resolution of $10'$, making them difficult to

correlate with high-resolution data in other spectral regimes. In this paper, it is possible for the first time to present a multiwavelength study of part of a composite remnant's shell at scales a small fraction of a parsec.

2. OBSERVATIONS

The Molonglo Observatory Synthesis Telescope (MOST) is an east-west multielement interferometer located in New South Wales, Australia (Robertson 1991). It consists of two co-linear cylindrical parabolas, each 11.6 by 778 m. In a 12 hr synthesis observation it images an elliptical field of size $70' \times 70'$ csc $|\delta|$.[1] Sixty-three of these synthesis observations covering an area of almost 50 deg^2 comprise this survey. The survey includes the regions of brightest radio emission from the Vela SNR and covers the majority of the X-ray remnant as seen by Aschenbach et al. (1995). The area close to the strong H II region RCW 38 has been avoided, due to imaging artifacts. Each observation was made at a frequency of 843 MHz and a resolution of $43'' \times 43''$ csc $|\delta|$, receiving right-handed circular polarization in a bandwidth of 3 MHz. The observations were made over the period 1984 February 3 to 1996 February 3. Complete coverage with the elliptical field shape necessitates substantial overlaps in the survey which have been used to refine the relative calibration between fields, based on the unresolved sources common to more than one field. Twenty-seven of the earlier observations were made for the First Epoch Molonglo Galactic Plane Survey (Whiteoak et al. 1989; Green et al. 1998), and some of these data appear in the MOST SNR Catalogue (Whiteoak & Green 1996). The remaining observations, which maintained the same basic grid separation of 0°.9, commenced on 1992 January 17.

Those observations initially made in the vicinity (within about 1°) of the Vela pulsar were severely limited in dynamic range by the presence of the pulsar in the primary beam. The pulsar is a strong, unresolved continuum source and is variable over timescales of seconds to hours. Its integrated pulsed emission in ungated observations was 2.2 ± 0.4 Jy, averaged over the entire pulsar period. A source will appear in a MOST image with a symmetric point-spread function only if its intensity remains constant throughout the observation. Any time-dependent variation compromises sidelobe cancellation during synthesis, producing rays within the image emanating from the source, and confusing nearby faint features. To improve the imaging of this region, a method of pulsar gating was used which was originally developed by J. E. Reynolds (1996, private communication) for an observation in 1986.

To make the observations, a predicted pulse arrival time was used to generate a gating signal of width 20 ms in each pulsar period ($\sim$89 ms).[2] This was displayed on an oscilloscope simultaneously with the actual detected total power signal of the pulsar. The half-power pulse width of the pulsar signal was 4.5 ms, larger than the observed half-power width of 2.3 ms at 632 MHz (McCulloch et al. 1978) due to the dispersion (2 ms) over the MOST's bandwidth (following Komesaroff, Hamilton, & Ables 1972) and to the effect of an integrating a low pass filter present in the signal path before the detection point. The gating signal was adjusted to suppress data acquisition from 5 ms before until 15 ms after the peak of the pulse, to allow removal of almost all of the variable pulsed emission. Four observations were made, each with the pulsar near the edge of the field to the north, south, east, and west. These observations were incorporated in the complete mosaic in place of the non-gated data, for this part of the survey. The observations made with this procedure contain only a 40 mJy (2%) residual of the pulsed emission, sufficient to preclude associated imaging artifacts. However, some artifacts are present in more remote fields, mainly due to the grating response of the MOST to the pulsar. Further details of the pulsar gating procedure are given by Bock (1997).

3. IMAGING

Individual images were synthesized from each of the 63 (12 hr) observations using the back-projection algorithm (Perley 1979; Crawford 1984) as implemented in the standard MOST reduction software. To provide initial calibration for the reduction process, several strong unresolved sources were observed briefly before and after each target observation. These provide a preliminary gain, phase, and beam-shape calibration. The images were deconvolved using the Högbom CLEAN algorithm. Some images containing stronger sources were adaptively deconvolved as described by Cram & Ye (1995). This method is similar to self-calibration, but with a reduced set of free parameters. The residual images had pixel rms in the range 1 to 6 mJy beam^{-1}. This range reflects the variation between fields that were essentially noise-limited and those that were dynamic-range limited.

Preliminary position and flux calibration used short observations of a number (typically eight) of unresolved calibration sources before and after each Vela target field. These sources are a subset of the MOST calibrators from Campbell-Wilson & Hunstead (1994). A refined calibration was achieved using unresolved survey field sources which are located in the overlapped regions. Measurement of these sources produced small corrections that result in positions mostly consistent to better than 1″ in right ascension and 2″ in declination and flux densities accurate to within 5%.[3] The refining corrections could not be applied to some fields that had too few unresolved sources in common with nearby fields (e.g., those at the edge of the mosaic). The individual fields were mosaicked into ARC projection (Greisen & Calabretta 1996), to facilitate comparison with optical surveys.

The MOST is a redundant array sensitive to the full range of spatial frequencies within the limits set by its extreme spacings. The minimum geometric spacing (42.85λ) implies a maximum detectable angular scale of about 1°.3. However, it has been found empirically that the actual synthesized beam of the MOST is best fit with a model including an effective minimum spacing of about 70λ. This parameter varies between and during observations. Typically, angular scales less than about 30′ are well imaged. The MOST's synthesized beam can also vary significantly

[1] Recent modifications have increased the field of view to $163' \times 163'$ csc $|\delta|$.

[2] The predicted pulse arrival time was determined from timing measurements of the pulsar kindly provided by R. N. Manchester (ATNF), M. Bailes (Univ. of Melbourne), and P. M. McCulloch (Univ. of Tasmania).

[3] The uncertainties in the absolute calibration of MOST images are approximately an additional 5% in flux density and 0″.5 in R.A. and decl. (Hunstead 1991, 1997, private communication).

during an observation due to environmental effects and minor telescope performance variations with the result that the theoretical beam used for deconvolution sometimes does not model well the actual beam of an observation. A combination of these effects produces a negative bowl artifact around bright extended sources. In the MOST Vela SNR survey, this effect causes a background level of about -10 mJy beam^{-1} around Vela X and Puppis A.

Extended structure at levels as low as 6 mJy beam^{-1} is clear in the images. Although the rms in individual pixels is around 2 mJy beam^{-1}, typical extended structure covers many pixels and is reliably detected at lower levels than would usually be accepted for point sources. The confirmation of this low-level structure in a VLA image of Vela X made at 1.4 GHz (Bock et al. 1998) validates similar emission seen at 843 MHz elsewhere in the survey.

The most common artifacts present in the image are grating rings, which are due to the periodic nature of the MOST. They are sections of ellipses of dimension $1\overset{\circ}{.}15 \times 1\overset{\circ}{.}15 \csc |\delta|$, with a width dependent on the source producing them, and are, in general, of variable amplitude since they pass through several individual fields where the grating rings have different relative gains. The morphology of these artifacts makes them easily distinguishable from the sky emission. Much of the survey is dynamic-range limited; in the less complicated regions the rms noise is of order 1–2 mJy beam^{-1}.

An additional nonideality comes from the mosaicking: the image from each of the 63 individual observations was deconvolved separately, yet structure outside a given field can contribute to sidelobes in that field. This manifests itself as discontinuities in the survey image, at the edges of component images, or where regions containing artifacts have been masked.

4. RESULTS

An image of the complete MOST survey of the Vela SNR is shown in Figure 1. To assist in identifying the various objects and emission regions within the survey, a cartoon covering the same area is presented in Figure 2. Key characteristics of the survey are summarized in Table 1.

Morphologically, there are several distinct regions apparent in the image. Near the center is the bright nebula known as Vela X, which is thought to be powered by the Vela pulsar (PSR B0833−45: Large, Vaughan, & Mills 1968). The nebula is composed of a network of complex filaments. Significant extended structure is also present but not detected by the MOST. This region is seen more clearly in subsequent images.

In the north and east of the image there are several filaments from the shell of the Vela SNR and at least one unrelated H II region, RCW 32 (Rodgers, Campbell, & Whiteoak 1960). There are also partial elliptical artifacts due to strong H II regions outside the survey area. Broadly speaking, we can categorize the extended structure in this area on morphological grounds. To the northeast of the Galactic plane, much of the structure is diffuse and randomly oriented and may be Galactic emission unrelated to the Vela SNR. Most of the extended emission between the Galactic plane and the Vela X nebula *is* due to the Vela supernova event. These filamentary features have some correspondence with optical filaments and X-ray emission in the area (§ 4.1). They are generally perpendicular to the direction to the center of the SNR and are presumably related to the shell. This is the area known in the literature as Vela Y (Dwarakanath 1991; Milne 1968a). Directly to the east of Vela X is the radio peak known as Vela Z. This area is confused by the elliptical sidelobe from the bright H II region RCW 38 (Rodgers et al. 1960), which is not included in the survey. The area around RCW 38 is included in the First Epoch Molonglo Galactic Plane Survey (Green et al. 1998). On the southern side of the central nebula, another region of shell-like emission ($08^{h}32^{m}$, $-49°00'$) is probably also part of the Vela SNR. This coincides approximately with the southern boundary of the 8° remnant (Aschenbach 1992; Duncan et al. 1996).

The survey contains many unresolved and barely resolved sources, most of which are presumably background sources.[4] However, some may be density enhancements in the Vela emission or other Galactic objects, such as compact H II regions, planetary nebulae, pulsars, or small-diameter SNRs. Several of these sources have unusual coincidences with extended structures. From the survey it is unclear whether they are, in fact, background sources, or whether they are "knots" in the SNR emission. Follow-up VLA observations (Bock et al. 1998) of four of these sources have not found evidence for a Galactic origin.

The unrelated supernova remnant Puppis A is also contained within the survey. It is an oxygen-rich SNR of age about 3700 yr (Winkler et al. 1988) at an accepted distance of 2 kpc (Arendt et al. 1990). Puppis A has previously been imaged separately with the MOST (Kesteven & Caswell 1987; Arendt et al. 1990). It falls approximately on the 8° X-ray boundary of the Vela SNR. However, no Vela radio emission is obvious in the vicinity.

TABLE 1

KEY PARAMETERS OF THE MOST VELA SNR SURVEY

Parameter	Value
Frequency	843 MHz
Bandwidth	3 MHz
Total area	50 deg^2
Individual field size ($\alpha \times \delta$)	$70' \times 70' \csc |\delta|$
Resolution ($\alpha \times \delta$)	$43'' \times 43'' \csc |\delta|$
Maximum imaged angular scale	$\sim 30'$
Typical rms noise	1–2 mJy beam^{-1}
Received polarization	Right circular (IEEE)

4.1. *The Northern Shell*

The present survey of the Vela SNR covers much of the brightest region of the Vela shell. The image in Figure 3 is part of the survey showing the northern section of the Vela SNR shell. The following discussion focuses on this area, where the radio emission from the shell is most prominent and not confused by emission from unrelated Galactic objects or by artifacts.

The extended structure in this image is in a series of filamentary arcs across the image at position angles ranging from 70° to 170°. The structure is generally concave toward the center of the SNR: there are no significant radial filaments. The majority of the filaments are resolved by the MOST, with widths ranging from $1'$ to $6'$ and peak surface brightnesses up to 20 mJy beam^{-1}. These filaments gener-

[4] About 39 small-diameter sources above 5 mJy at 843 MHz are found per square degree away from the Galactic plane (Large et al. 1994).

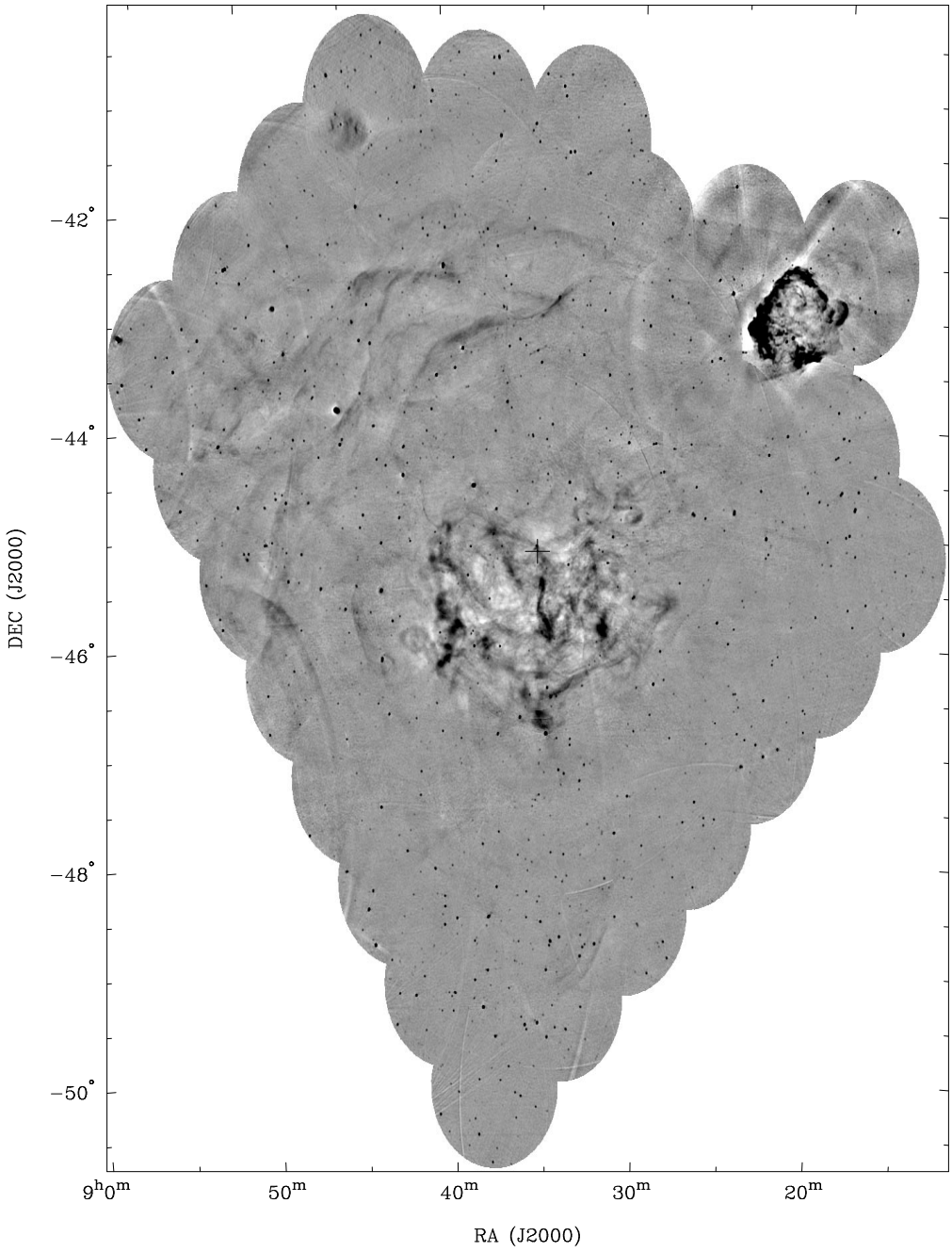

FIG. 1.—The 843 MHz survey of the Vela SNR. Vela X is the central, nebulous region composed of many filaments in an area about 2° across, centered on 08^h35^m, −45°30′, with the Vela pulsar (suppressed in this image) offset from the center of the nebula at a position marked with a cross. The radio shell can be seen most clearly around 08^h42^m, −43°00′. The separate SNR, Puppis A, is also included in the survey, at 08^h22^m, −43°00′. The gray-scale image is saturated outside the intensity range of −20 to 30 mJy beam^{-1} to show the extended structure most clearly.

ally have a sharp edge on the side away from the center of the remnant, while toward the remnant center they may fade over several arcminutes. The sharper outside profile is consistent with the "projected sheet" picture of filamentary emission (Hester 1987). The effect may also indicate that the filaments are in fact edges, spatially filtered by the MOST so that only the sharp transitions appear.

4.1.1. *A Multiwavelength Comparison*

The availability of three data sets of comparable resolution at widely spaced wavelengths gives us an opportunity to understand the spatial relationship between the underlying physical processes. In addition to the 843 MHz survey with the MOST, Hα and soft X-ray data are available. The radio image shows primarily the nonthermal synchrotron emission, the optical filaments are line emission resulting from recombination in cooling processes, while the X-rays are shock heated thermal radiation.

An Hα image of the northern Vela shell is shown in Figure 4*a*, overlaid with a contour (at approximately the 3 σ level) from the radio image of Figure 3. This image is from a test observation (kindly made and reduced by M. S. Bessell) for the Mount Stromlo and Siding Spring Observatories (MSSSO) Wide Field CCD Hα Imaging Survey (Buxton, Bessell, & Watson 1998). The observation was made using a 2048 × 2048 24 μm pixel CCD through a 400 mm, f/4.5

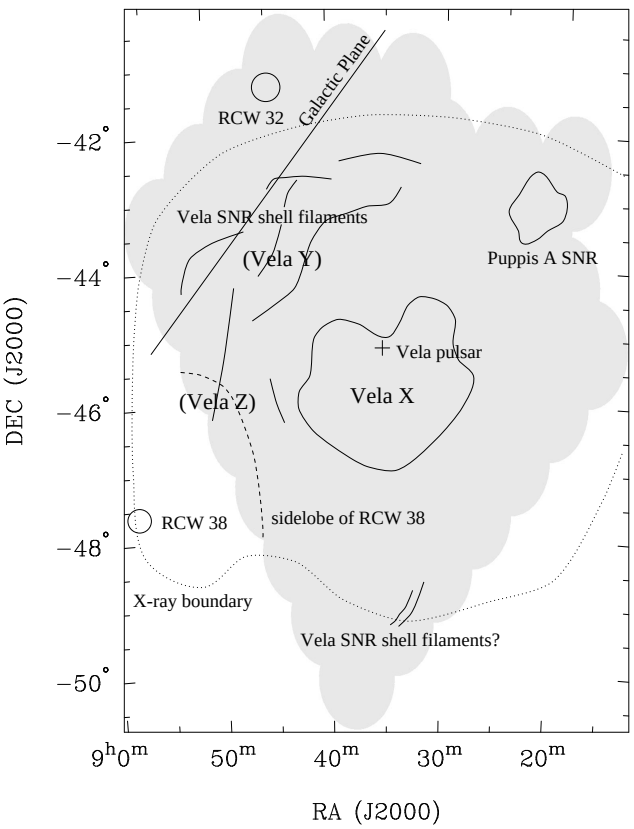

FIG. 2.—Cartoon of the same area as Fig. 1, showing key features in the region. The radio peaks (in total power observations) of Vela X, Y, and Z are marked at the positions adopted in the literature (Dwarakanath 1991; Milne 1968a). The names Vela Y and Z are superseded now that these regions have been resolved to show the filamentary structure. The approximate boundary of the X-ray remnant (Aschenbach et al. 1995) is marked with a dotted line.

Nikkor-Q lens, at the 16 inch (0.4 m) telescope facility at Siding Springs Observatory. Pixel spacing in the image is 12″, giving a field size of 7 deg^2. The portion of this image presented here is taken from the central (5° × 5°) region, where vignetting in the 1.5 nm filter is not significant. The image has been derived from two frames with a total exposure time of 1400 s, which were bias-subtracted and flat-field corrected before averaging. No correction has been made for the effect of cosmic rays. No continuum observation was made for subtraction. Consequently, the image presented here contains stars and a continuum component in the extended emission. A coordinate system was applied to the image by comparison with a Digital Sky Survey image (Morrison 1995) using the KARMA package (Gooch 1996). The registration is within the resolution of the radio data.

The Vela SNR was observed as part of the *ROSAT* All-sky Survey between 1990 October and 1991 January. An image of the Vela SNR (0.1–2.4 keV, with angular resolution 1′) from the survey has been presented by Aschenbach et al. (1995), and part is reproduced in Figure 4*b*, overlaid with the same radio contour as in Figure 4*a*. In the figure, the top section of the X-ray image (*black*) is the Galactic background. The surface brightness at the edge of the SNR shell is 7×10^{-15} ergs cm^{-2} s^{-1} arcmin^{-2} (Aschenbach et al. 1995). To the south, the surface brightness increases by a factor of 500 to the brightest part (*white*), which is the most intense X-ray–emission region in the entire SNR. The first gray area ($\delta = -41°40'$) marks the edge of the main shock, seen in projection.

4.1.2. *Morphological Analysis*

By considering only the radio and Hα images (Fig. 4*a*), it is possible to see immediately the most striking aspect of the comparison, namely, the contrast between the optical and radio emission regions. As will be discussed below, this has a simple theoretical basis, but is contrary to the picture seen in other SNRs in those cases where optical emission has been compared with well-resolved radio shell structure. The brightest radio filaments are (as noted earlier) generally oriented perpendicularly to the direction to the SNR center and are without optical counterparts. Likewise, many of the optical filaments are without radio counterparts. However, one of the brightest optical filaments (with orientation similar to the radio structures), centered on 08^{h}36^m, −42°50′, does have a faint radio counterpart. By contrast, the equally bright optical filaments in the southwest corner of the image are without radio counterparts in the MOST image. These filaments are generally not oriented perpendicularly to the direction to the SNR center in the same way as the radio filaments.

In addition to the optical filamentary structure, diffuse optical emission is also present. This is concentrated to the eastern side of the image, in the general area of the strong radio filaments, but there is no obvious correlation between the diffuse optical emission and the radio filaments. No direct measure of the effect of extinction on the Hα image is available.

The complete X-ray image (Aschenbach et al. 1995) shows by its near-circular shape that it delineates the projected edge of those parts of the main shock that are still expanding into a relatively homogeneous medium. The regions of optical and radio emission described so far are interior to this main X-ray shell. At the western side of the main X-ray boundary in Figure 4*b*, we see significant optical and radio emission clearly present close to the X-ray edge. Here the radio and optical emission agree quite well, in an arc with apex at 08^{h}35^m, −42°10′, just behind the outer edge of the X-ray emission.

The X-ray emission is quite different in form to the emission we see in the optical and radio regimes. Apart from the main edge, it is relatively diffuse and smooth. By contrast, the radio and optical images are dominated by filamentary structure. However, we note that the radio image has reduced sensitivity to smooth structure, due to the MOST's spatial response.

The bright optical filament at 08^{h}36^m, −42°50′ traces the exterior (with respect to the remnant expansion) of the brightest peaks of the X-ray emission. Yet not all the optical filaments exhibit this relationship. The diffuse optical component has no obvious X-ray counterpart and is strongest where the X-ray emission is not quite so bright, to the east. The radio filaments are also partially correlated with the X-ray emission. Several follow changes in X-ray brightness. However, the most central filament (08^{h}39^m, −43°10′) is less well correlated: it crosses a bright region of X-ray emission.

4.1.3. *Radiation Mechanisms*

In SNRs, optical and X-ray emission are both typically due to thermal processes. However, quite different physical conditions are involved. Thermal X-ray emission is the result of fast shocks propagating through a rarefied

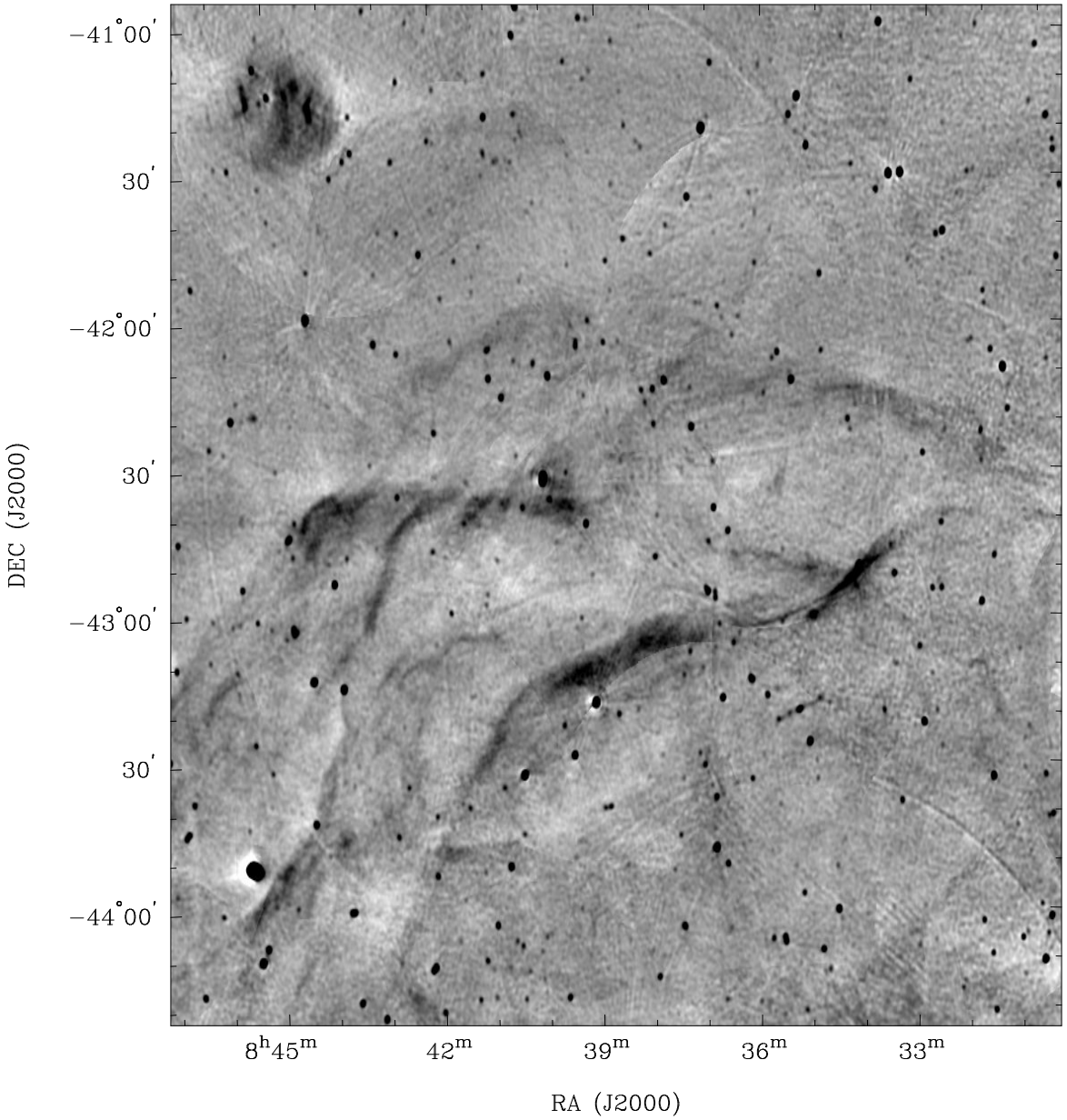

FIG. 3.—Subimage of Fig. 1, showing the northern radio continuum (843 MHz) filaments. The intensity scale is linear, from −10 (*white*) to 15 (*black*) mJy beam^{-1}.

medium, with density 0.1–1 cm^{-3}, shocked to temperatures of 10^6–10^7 K (Lozinskaya 1992). The optical emission typically observed is produced by hydrogen recombination of cooling shocked gas at about 10^4 K, with density a few times 10^2 cm^{-3}.

One model that has had success explaining optical and X-ray observations of the Cygnus Loop (Hester & Cox 1986; Graham et al. 1995; Levenson et al. 1996) invokes large ($\gtrsim 10^{14}$ m) molecular clouds with which the expanding shock is interacting. The optical emission comes from the shocked cloud, where the dense material is not heated to temperatures as high as those which are maintained in the less dense X-ray–emitting regions. This emission is a result of recombinative cooling after the passage of the shock. Behind the optical emission, the X-ray emission is further brightened by the passage of a reflected (or reverse) shock due to the density contrast between the cloud and the less dense intercloud material. Where the main shock does not encounter molecular clouds, we do not expect to see recombinative cooling. Instead the nonradiative shock may be traced by fainter Balmer filaments (Hester, Raymond, & Blair 1994).

The present observations of the northern Vela shell fit nicely into this picture. If the majority of optical emission was from the main shock interacting with a relatively uniform medium, but seen here in projection, we would expect also to see it along the entire edge of the X-ray shell, where accentuation of sheetlike emission in projection would be strongest. This is not observed, implying the emission is localized and due to some interaction in density inhomogeneities with a filling factor much less than unity. The cloud interaction model is further supported by the presence of X-ray–brightened regions (Fig. 4*b*) immediately behind the bright optical filamentary structure centered on 08^h36^m, −42°50′ in Figure 4*a*. We might be seeing this emission in projection, significantly in front of or behind the

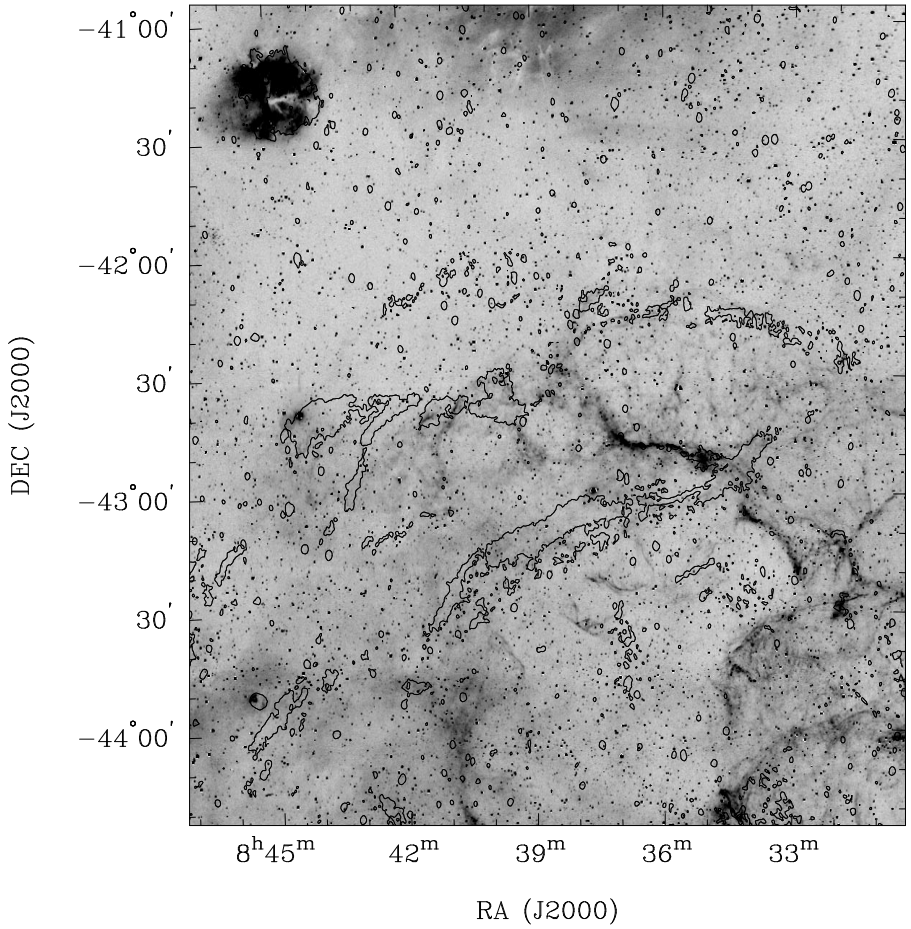

FIG. 4*a*

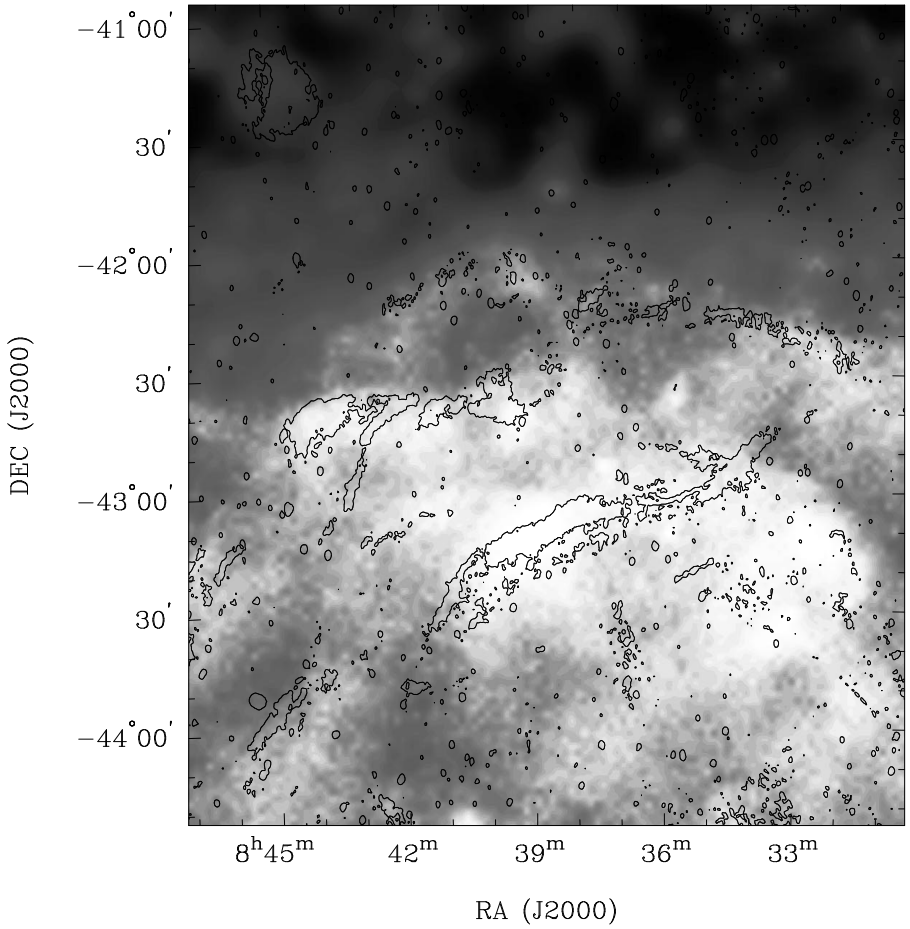

FIG. 4*b*

FIG. 4.—Single 843 MHz contour (at 4 mJy beam^{-1}) on (*a*) Hα and (*b*) X-ray images. The Hα image is from the MSSSO Hα Survey (Buxton et al. 1998), courtesy of M. S. Bessell. The X-ray image was kindly provided by B. Aschenbach (originally published in Aschenbach et al. 1995).

plane of the explosion center transverse to the line of sight. This would indicate local density enhancements very close to the main shock. Alternatively, it could be nearly in the plane of the explosion center, with a shock velocity significantly reduced by interactions with more dense material. Some of the emission could be from regions already passed and energized by the main shock.

The digital 60 μm images in the *IRAS* Sky Survey Atlas (Wheelock et al. 1994) support the thermal emission model for the X-ray emission. Much of the X-ray structure does have an infrared counterpart. However, infrared images are generally less useful thermal diagnostics than X-ray images near the Galactic plane, since the infrared observations are dominated by diffuse Galactic emission and confusion from other sources (White & Long 1991).

An alternative model for SNR optical/X-ray emission (McKee & Cowie 1975) explains SNRs with centrally-peaked X-ray emission (White & Long 1991). In this model cold dense clouds with a small filling factor have been passed by the main shock and are evaporating by conductive heating from the postshock gas.

Both these models rely on molecular clouds to explain the observed features. Molecular clouds have been detected in the direction of the Vela SNR (May, Murphy, & Thaddeus 1988). The initial survey was of ^{12}CO and ^{13}CO $J = 1 \rightarrow 0$ line emission with a resolution of 0.°5. Higher resolution follow-up observations (Murphy & May 1991) covered only the eastern part of the Vela SNR shell. A cloud with a barely resolved peak at $08^{h}41^{m}$, $-41°20'$ is seen, with a distance estimated to be 0.5–2.0 kpc, i.e., immediately behind the Vela SNR. However, this cloud appears coincident with a bright H II region seen optically to the north of Figure 4*a* and might not be responsible for the observed optical features in the Vela shell. H I may be a better tracer of density in the Vela shell region. Dubner et al. (1998) find a near-circular shell of H I surrounding the northern edge of the remnant, with column densities up to 10^{21} cm^{-2}, and estimate the preshock gas to have had a density of 1–2 cm^{-3}. The H I shell traces the X-ray edge of the remnant, enclosing the radio and optical filaments.

In the simple radio emission model for the interaction of supernova explosions with the ISM (Woltjer 1972), Vela is in the radiative or snowplow phase of evolution, having swept up significant matter and dissipated much of the original kinetic energy of the explosion. A cool dense shell surrounds a hot interior. This model can account for the faint radio emission seen just behind the X-ray edge, which indicates the presence of compressed magnetic fields and accelerated particles, probably from the diffusive shock mechanism (Fulbright & Reynolds 1990). It does not account for the brighter localized filaments apparently well behind the main shock.

Duin & Van Der Laan (1975) present a consistent picture for the coincidence of radio and optical emission that is observed in "middle-aged" shell remnants. This model, based on observations of IC443, proposes that the magnetic field required for synchrotron emission is frozen into condensations forming in the cooling instabilities which then give rise to the optical emission. We do not find significant radio/optical coincidence in our Vela observations. Consequently, if this process is occurring, then we can infer that the cooling material around the radio filaments is not at an appropriate temperature for the emission of recombination radiation. One explanation is for a long period to have elapsed following the passage of the radiative shock, allowing substantial cooling while still preserving the conditions for synchrotron emission (Blandford & Cowie 1982). Alternatively, where shock-accelerated particles producing the optical filaments are located, the magnetic field may not be sufficiently compressed to cause detectable synchrotron emission.

The applicability of these models may be investigated further with magnetic field information, provided by polarimetry. Polarized intensity has been observed in the Vela shell (Duncan et al. 1996), but high-resolution measurements at several frequencies will be required to examine the magnetic field structure in this area in detail. Blandford & Cowie (1982) note that individual filaments ought to be polarized parallel to their longest dimensions, although they may be too faint to be detected with current instruments.

Good agreement between optical and radio emission has been found in other middle-aged shell SNRs such as IC443 (Duin & Van Der Laan 1975), the Cygnus Loop (Straka et al. 1986), and HB3 (Fesen et al. 1995). The situation in Vela is quite different, and the reason for this is not apparent. Extinction may be a culprit, obscuring some of the Hα emission. However, the coincidence of diffuse optical emission with bright radio filaments, noted above, argues against massive extinction in this direction.

This initial investigation of the optical/radio/X-ray correlations in the region indicates that a fuller investigation would be profitable. A first step would be to obtain optical spectral information to separate nonradiative and radiative filaments, allowing a detailed comparison with the model of Hester & Cox (1986).

4.2. *Vela X*

A view of the central nebula of the Vela SNR is shown as a gray-scale image in Figure 5 and as a ruled surface plot in Figure 6. Each representation emphasizes different characteristics. The gray-scale image gives a good overall view of the region, while the ruled surface plot helps to show the nature of the filamentary structure and highlights the small-diameter sources.

The first thing to note in the images is that at the resolution of these observations the nebula is seen to be composed of many filaments or wisps, at a variety of orientations and on many angular scales. Several of the brighter filaments are aligned approximately north-south. It is important to realize that the flux density detected in this image is only a small fraction of the total flux density of the remnant, because of absent low spatial frequency information. The total flux density of the extended features in the MOST image of Vela X is calculated to be 28 ± 2 Jy, which becomes 130 Jy when correction is made for the negative bowl artifact surrounding the nebula. This is approximately 12% of the estimated single-dish flux density of Vela X (Dwarakanath 1991). One benefit of the MOST acting as a spatial filter is the prominence it gives to smaller scale structures with size of the order of the X-ray feature seen by Markwardt & Ögelman (1995). In Figure 5, the central radio filament overlaid on the X-ray feature by Frail et al. (1997) is marked "1." This filament does not look strikingly different from other filaments in the region, e.g., the filament marked "2." However, we see in the 8.4 GHz Parkes image of Milne (1995) that filament "1" is located at the brightest part of the Vela X nebula. Frail et al. (1997) have argued

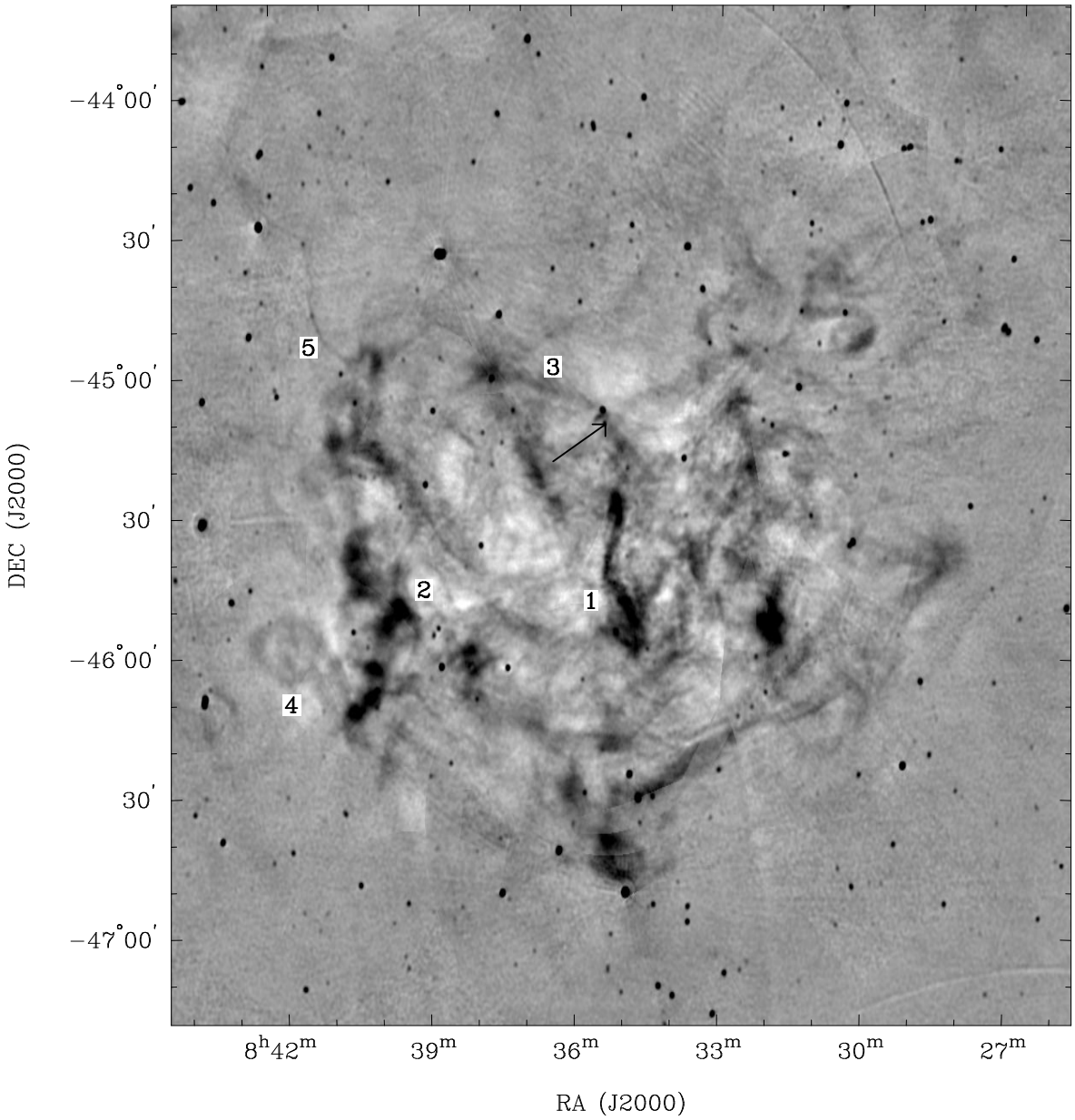

FIG. 5.—Subimage of Fig. 1, showing Vela X, the central nebula of the Vela SNR. The arrow shows the direction and magnitude of the proper motion of the pulsar over 12,000 yr, assuming constant velocity as measured by Bailes et al. (1989). The arrow's head is at the present location of the pulsar (suppressed in this image). The numbers refer to features discussed in the text.

that this radio filament may be associated with the X-ray feature, but it is morphologically indistinguishable from other filaments in the image. The central radio filament looks so prominent in the 327 MHz VLA image of Frail el al. (1997) partially because that image is uncorrected for the VLA primary beam attenuation at the edge of the field. Also, the maximum entropy method of deconvolution used for the VLA data promotes the flux density at low spatial frequencies more than the CLEAN algorithm used to deconvolve the MOST observations.

Several further interesting objects in the region should be noted. In Figure 5, a filament ("3") extends through the pulsar position (at the head of the arrow) to the south and may connect to filament "1." The axis of symmetry of these two filaments is closely aligned with the direction of motion of the pulsar (Bailes et al. 1989), shown on the image with an arrow. Using the proper motion measurement of Bailes et al. (1989), we notice that over its lifetime (assuming an age of 12,000 yr) the pulsar has moved to its present position from a bright region to the southeast. An excess of high-energy γ-rays has been detected from near this putative birthplace (Yoshikoshi et al. 1997). Greater age estimates (e.g., Aschenbach et al. 1995; Lyne et al. 1996) change this slightly as they increase the distance moved by the pulsar by up to a factor of 2. Just to the north of the pulsar is a 3′ crescent-shaped synchrotron nebula, seen originally by Bietenholz, Frail, & Hankins (1991). They resolved out the extended structure in the region, whereas here we see that the crescent is one bright region of much extended emission around the pulsar. Some very faint structures found around the edge of Vela X appear unusual. Object "4" has a shape reminiscent of many shell supernova remnants, but if it is associated with Vela X, it might be a blowout from the nebula. Object "5" is a faint streamer apparently connect-

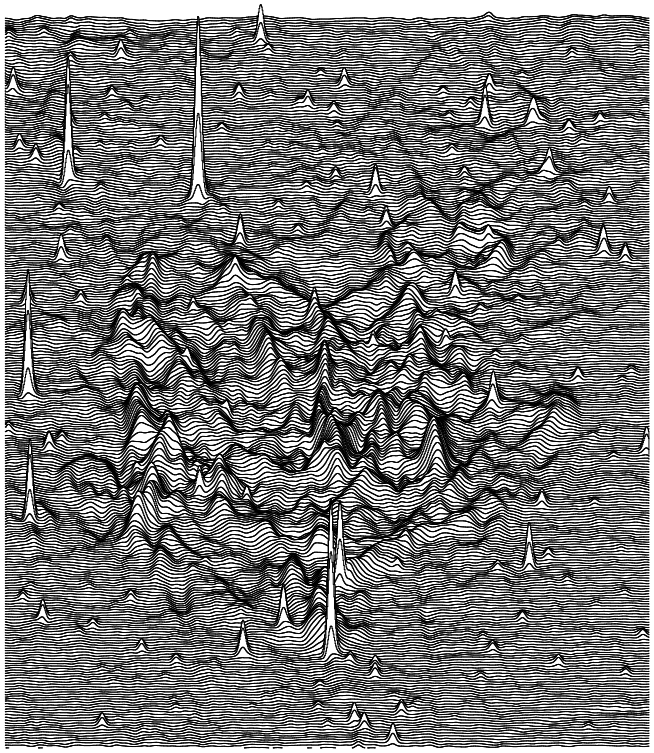

FIG. 6.—Ruled surface plot of the same area as Fig. 5, emphasizing the disordered nebulosity of Vela X and highlighting the relative strengths of the point sources and the extended structure. The data have been convolved to a circular beam of 120″ × 120″ to reduce the noise, which also accentuates the extended emission (by a factor of 5.6) relative to the compact sources.

ing Vela X to the Vela shell (cf. Fig. 1). It might be argued that this is actually a foreground or background projection of the surface of a shock "bubble," but it is substantially thinner than any of the shell filaments.

5. CONCLUSION

The radio survey presented in this paper contains the highest resolution observations yet made of the bulk of the Vela supernova remnant (SNR) and resolves the structure of the remnant in more detail than has been possible for any other composite remnant. The resolution of this observation of the Vela X region is a factor of 2 greater than that presented by Frail et al. (1997) and covers the entire plerion, unaffected by primary beam attenuation. The Vela plerion in the radio consists of both diffuse and filamentary emission. Although the survey does not contain information on the largest spatial scales, this structure may be inferred from single-dish observations at higher frequencies (Milne 1995; Duncan et al. 1996), which show that the filamentary emission in the survey covers the same area as the more diffuse emission from Vela X seen in total power images. The region immediately surrounding the Vela pulsar contains more nonthermal emission in addition to the possible pulsar wind nebula seen by Bietenholz et al. (1991).

The two distinct regions of the Vela SNR, the shell and the plerion, have in the past been considered separate entities because of their different spectral indices. This characteristic puts Vela in the composite class with SNRs such as G326.3−1.8 (MSH 15–56: Clark, Green, & Caswell 1975; Whiteoak & Green 1996) and G0.9 + 0.1 (Helfand & Becker 1987). In the images presented in this paper, we now see the shell and plerion in fine detail, and they separately show strong similarities with what we see in other SNRs, observed at similar resolutions. The shell filaments are comparable to those seen in the Cygnus Loop (Green 1984; Straka et al. 1986), oriented perpendicularly to the direction to the SNR center, with Hα and X-ray counterparts. By contrast, the filamentary structure within the plerion is more nebulous and has a gross alignment approximately north-south. Its appearance is reminiscent of the filaments in the Crab Nebula (Bietenholz & Kronberg 1990). Thus we can identify both a shell and a plerion within the Vela SNR, classifying it unambiguously as a composite remnant.

We propose that it be considered as the archetypal Galactic member of the composite class. In angular extent, the Vela SNR is respectively 50 and 12 times larger than G0.9 + 0.1 and G326.3−1.8, allowing detailed studies at a variety of wavelengths. It is now appropriate to use this object as a key laboratory for studying the properties of SNRs and the interstellar medium.

The investigation of the shell of the Vela SNR in this paper focused on its northern side. Like parts of the Cygnus Loop, this region can be explained by a model of a fast shock heating interstellar material to X-ray–emitting temperatures and interacting with denser clouds to produce Hα recombination line emission (Hester & Cox 1986; Graham et al. 1995; Levenson et al. 1996). The expanding shock also produces bright nonthermal radio emission not well correlated with these Hα filaments, in contrast with the optical/radio agreement seen in many other middle-aged SNRs. To continue investigating this region, observations of other optical emission lines are needed to separate projected Balmer filaments, produced at the outer shock, from recombination line emission at molecular cloud interactions. High-resolution polarization observations of the radio shell filaments are the obvious next step to investigate the magnetic field associated with the nonthermal emission.

Further study of the remnant's plerionic component, Vela X, should determine how the Vela pulsar transfers its rotational kinetic energy to the nebula. With an age at least 10 times that of the Crab Nebula, we might expect the Vela plerion to show evolutionary trends in the relative emission strengths in different wavelength regimes. The absence of obvious correlations between radio emission and the optical filaments (Elliott, Goudis, & Meaburn 1976) already contrasts Vela X with the Crab Nebula, where the radio filaments surround the optical filaments (Wright & Foster 1980). The recent discovery of a possible X-ray "jet," which might be the conduit for energy transfer to the nebula from the pulsar (Markwardt & Ögelman 1995), further contrasts Vela X with other plerions currently known.

The Molonglo Observatory Synthesis Telescope is operated by the School of Physics, with funds from the Australian Research Council and the Science Foundation for Physics within the University of Sydney. The authors thank D. A. Frail for useful discussions in the course of this work; J. E. Reynolds for assistance with the pulsar gating observations; B. Aschenbach and M. S. Bessell for providing electronic versions of their images; and M. Bailes, P. M. McCulloch, and R. N. Manchester for providing Vela pulsar timing data. D. C.-J. B. also acknowledges financial support from an Australian Postgraduate Award while at the University of Sydney.

REFERENCES

Arendt, R. G., Dwek, E., Petre, R., Dickel, J. R., Roger, R. S., Milne, D. K., & Kesteven, M. J. 1990, ApJ, 350, 266
Aschenbach, B. 1992, in Space Science with Particular Emphasis on High Energy Astrophysics, ed. J. Trümper (Garching bei München: Max-Planck-Institut für Extraterrestriche Physik), 28
Aschenbach, B., Egger, R., & Trümper, J. 1995, Nature, 373, 587
Bailes, M., Manchester, R. N., Kesteven, M. J., Norris, R. P., & Reynolds, J. E. 1989, ApJ, 343, L53
Bietenholz, M. F., & Kronberg, P. P. 1990, ApJ, 357, L13
Bietenholz, M. F., Frail, D. A., & Hankins, T. H. 1991, ApJ, 376, L41
Blandford, R. D., & Cowie, L. L. 1982, ApJ, 260, 625
Bock, D. C.-J. 1997, Wide Field Aperture Synthesis Radio Astronomy, Ph.D. thesis, Univ. Sydney
Bock, D. C.-J., Frail, D. A., Sault, R. J., Green, A. J., & Milne, D. K. 1998, in preparation
Buxton, M., Bessell, M., & Watson, B. 1998, Publ. Astron. Soc. Australia, 15, 24
Campbell-Wilson, D., & Hunstead, R. W. 1994, Proc. Astron. Soc. Australia, 11, 33
Clark, D. H., Green, A. J., & Caswell, J. L. 1975, Australian J. Phys. Astrophys. Suppl., 37, 75
Cram, L. E., & Ye, T. 1995, Australian J. Phys., 48, 113
Crawford, D. F. 1984, in Indirect Imaging, ed. J. A. Roberts (Cambridge: Cambridge Univ. Press), 373
Day, G. A., Caswell, J. L., & Cooke, D. J. 1972, Aust. J. Phys. Astrophys. Suppl., 25, 1
Dubner, G. M., Green, A. J., Goss, W. M., Bock, D. C.-J., & Giacani, E. 1998, AJ, 116, 1842
Duin, R. M., & Van Der Laan, H. 1975, A&A, 40, 111
Duncan, A. R., Stewart, R. T., Haynes, R. F., & Jones, K. L. 1996, MNRAS, 280, 252
Dwarakanath, K. S. 1991, J. Astrophys. Astron., 12, 199
Elliott, K. H., Goudis, C., & Meaburn, J. 1976, MNRAS, 175, 605
Fesen, R. A., Downes, R. A., Wallace, D., & Normandeau, M. 1995, AJ, 110, 2876
Frail, D. A., Bietenholz, M. F., Markwardt, C. B., & Ögelman, H. 1997, ApJ, 475, 224
Fulbright, M. S., & Reynolds, S. P. 1990, ApJ, 357, 591
Gooch, R., 1996, in Astronomical Data Analysis Software and Systems V, ed. G. H. Jacoby & J. Barnes (San Francisco: ASP), 80
Graham, J. R., Levenson, N. A., Hester, J. J., Raymond, J. C., & Petre, R. 1995, ApJ, 444, 787
Green, A. J., Cram, L. E., Large, M. I., & Ye, T. 1998, ApJ, submitted
Green, D. A. 1984, MNRAS, 211, 433
Greisen, E. W., & Calabretta, M. 1996, Representations of Celestial Coordinates in FITS, unpublished
Gum, C. 1955, MmRAS, 67, 155
Haslam, C. G. T., Stoffel, H., Salter, C. J., & Wilson, W. E. 1982, A&AS, 47, 1
Helfand, D. J., & Becker, R. H. 1987, ApJ, 314, 203
Hester, J. J, 1987, ApJ, 314, 187
Hester, J. J., & Cox, D. P. 1986, ApJ, 300, 675
Hester, J. J., Raymond, J. C., & Blair, W. P. 1994, ApJ, 420, 721
Kaspi, V. M. 1996, in Pulsars: Problems & Progress, ed. S. Johnston, M. A. Walker, & M. Bailes (San Francisco: ASP), 375
Kesteven, M. J., & Caswell, J. L. 1987, A&A, 183, 118
Komesaroff, M. M., Hamilton, P. A., & Ables, J. G. 1972, Australian J. Phys., 25, 759
Kundt, W. 1988, in Supernova Shells and Their Birth Events, ed. W. Kundt (Berlin: Springer-Verlag), 1
Large, M. I., Vaughan, A. E., & Mills, B. Y. 1968, Nature, 220, 340
Large, M. I., Campbell-Wilson, D., Cram, L. E., Davison, R. G., & Robertson, J. G. 1994, Proc. Astron. Soc. Australia, 11, 44
Levenson, N. A., Graham, J. R., Hester, J. J., & Petre, R. 1996, ApJ, 468, 323
Lozinskaya, T. A. 1992, Supernovae and Stellar Wind in the Interstellar Medium (New York: AIP), chap. 8
Lyne, A. G., Pritchard, R. S., Graham-Smith, F., & Camilo, F. 1996, Nature, 381, 497
Markwardt, C. B., & Ögelman, H. 1995, Nature, 375, 40
May, J., Murphy, D. C., & Thaddeus, P. 1988, A&AS, 73, 51
McCulloch, P. M., Hamilton, P. A., Manchester, R. N., & Ables, J. G. 1978, MNRAS, 183, 645
McKee, C. F., & Cowie, L. L. 1975, ApJ, 195, 715
Milne, D. K. 1968a, Australian J. Phys., 21, 201
———. 1968b, Australian J. Phys., 21, 501
———. 1980, A&A, 81, 293
———. 1995, MNRAS, 277, 1435
Milne, D. K., & Manchester, R. N. 1986, A&A, 167, 117
Morrison, J. E. 1995, in Astronomical Data Analysis Software and Systems IV, ed. R. A. Shaw, H. E. Payne, & J. J. E. Hayes (San Francisco: ASP), 179
Murphy, D. C., & May, J. 1991, A&A, 247, 202
Perley, R. A. 1979, AJ, 84, 1443
Reichley, P. E., Downs, G. S., & Morris, G. A. 1970, ApJ, 159, L35
Robertson, J. G. 1991, Australian J. Phys., 44, 729
Rodgers, A. W., Campbell, C. T., & Whiteoak, J. B. 1960, MNRAS, 121, 103
Stothers, R. 1980, PASP, 92, 145
Straka, W. C., Dickel, J. R., Blair, W. P., & Fesen, R. A. 1986, ApJ, 306, 266
Weiler, K. W., & Panagia, N. 1980, A&A, 90, 269
Weiler, K. W., & Sramek, R. A. 1988, ARA&A, 26, 295
Wheelock, S. L., et al. 1994, Sky Survey Atlas Explanatory Supplement, JPL Publication 94-11 (Pasadena: JPL)
White, R. L., & Long, K. S. 1991, ApJ, 373, 543
Whiteoak, J. B. Z., & Green, A. J. 1996, A&AS, 118, 329
Whiteoak, J. B. Z., Large, M. I., Cram, L. E., & Piestryzynski, B. 1989, Proc. Astron. Soc. Australia, 8, 176
Winkler, P. F., Tuttle, J. H., Kirshner, R. P., & Irwin, M. J. 1988, in Supernova Remnants and the Interstellar Medium, ed. R. S. Roger & T. L. Landecker (Cambridge: Cambridge Univ. Press), 65
Wright, M. C. H., & Forster, J. R. 1980, ApJ, 239, 873
Woltjer, L. 1972, ARA&A, 10, 129
Yoshikoshi, T., et al. 1997, ApJ, 487, L65